2D-NMR and ATR-FTIR Study of the Structure of a Cell-Selective Diastereomer of Melittin and Its Orientation in Phospholipids†

Michal Sharon,‡ Ziv Oren,§ Yechiel Shai,§ and Jacob Anglister*,‡

Department of Structural Biology and Department of Biological Chemistry, The Weizmann Institute of Science, Rehovot 76100, Israel

Received May 28, 1999; Revised Manuscript Received September 10, 1999

ABSTRACT: Melittin, a 26 residue, non-cell-selective cytolytic peptide, is the major component of the venom of the honey bee *Apis mellifera*. In a previous study, a diastereomer ([D]-$V^{5,8}$,I^{17},K^{21}-melittin, D-amino acids at positions $V^{5,8}$,I^{17},K^{21}) of melittin was synthesized and its function was investigated [Oren, Z., and Shai, Y. (1997) *Biochemistry 36*, 1826−1835]. [D]-$V^{5,8}$,I^{17},K^{21}-melittin lost its cytotoxic effects on mammalian cells; however, it retained antibacterial activity. Furthermore, [D]-$V^{5,8}$,I^{17},K^{21}-melittin binds strongly and destabilizes only negatively charged phospholipid vesicles, in contrast to native melittin, which binds strongly also zwitterionic phospholipids. To understand the differences in the properties of melittin and its diastereomer, 2D-NMR experiments were carried out with [D]-$V^{5,8}$,I^{17},K^{21}-melittin, and polarized attenuated total reflectance Fourier transform infrared (ATR-FTIR) spectroscopy experiments were done with both melittin and [D]-$V^{5,8}$,I^{17},K^{21}-melittin. The structure of the diastereomer was characterized by NMR in water, as well as in three different membrane-mimicking environment, 40% 2,2,2-trifluoroethanol (TFE)/water, methanol, and dodecylphosphocholine/phosphatidylglycerol (DPC/DMPG) micelles. The NMR data revealed an amphipathic α-helix only in the C-terminal region of the diastereomer in TFE/water and methanol solutions and in DPC/DMPG micelles. ATR-FTIR experiments revealed that melittin and [D]-$V^{5,8}$,I^{17},K^{21}-melittin are oriented parallel to the membrane surface. This study indicates the role of secondary structure formation in selective cytolytic activity of [D]-$V^{5,8}$,I^{17},K^{21}-melittin. While the N-terminal helical structure is not required for the cytolytic activity toward negatively charged membranes and bacterial cells, it appears to be a crucial structural element for binding and insertion into zwitterionic membranes and for hemolytic activity.

Melittin, a 26-residue highly basic, amphipathic polypeptide (GIGAVLKVLTTGLPALISWIKRKRQQ-$CONH_2$), is the major component of the honey bee (*Apis mellifera)* venom (*1*), and is one of the most studied membrane-seeking polypeptides (*2*). Melittin possesses various biological activities on membranes of different cells (for a review, see refs *2* and *3*), i.e., lysis of mammalian cells (*4, 5*), lysis of bacteria (*6, 7*), membrane fusion (*8, 9*), and activation of phospholipase A_2 (*10*). These effects of melittin result from its nonspecific interaction with a wide variety of membranes (*11*−*16*).

A large number of studies have been undertaken to determine the conformational properties of melittin, with the aim of understanding the molecular mechanism of melittin's interaction with membranes. Depending on the peptide concentration, pH, ionic strength, and the nature of the negative counterion, melittin is either monomeric in aqueous solution or associated as tetrameric aggregates (*17*−*22*). The aqueous monomer has no detectable secondary structure, as determined by circular dichroism (*19, 23, 24*) and ^{1}H NMR[1] (*20*). The X-ray structure of tetrameric melittin crystallized from aqueous solution (*25*) as well as the NMR structures of melittin in methanolic solution (*26*) and dodecylphosphocholine micelles (*27*−*30*) all indicate that the molecule consists of two α-helical segments (residues 2−10 and 13−26). These segments are connected by a hinge (residues 11 and 12) to form a bent α-helical rod with the hydrophilic and hydrophobic sides facing opposite directions. The conformation of melittin when bound to perdeuterated dipalmitoylglycerophosphocholine vesicles, was determined

† This work was supported by grants from the U.S.A-Israel Binational Science Foundation (Grant 95-246 to J.A.)

* To whom correspondence should be addressed. Phone: 972-8-9343394. Fax: 972-8-9344136.

‡ Department of Structural Biology.

§ Department of Biological Chemistry.

[1] Abbreviations: ATR-FTIR, attenuated total reflectance Fourier transform Infrared; CD, circular dichroism; COSY, 2D J-correlated spectroscopy; DMPG, 1,2 dimyristoyl-sn-glycerol-3-d_{54}; DPC, dodecylphosphocholine; HOHAHA, homonuclear Hartmann Hahn 2D experiment; NMR, nuclear magnetic resonance; NOE, nuclear Overhauser enhancement; NOESY, 2D NOE spectroscopy; PC, egg phosphatidylcholine; PG, egg phosphatidylglycerol; ROESY, rotating-frame Overhauser enhancement spectroscopy; RP-HPLC, reversed-phase high-performance liquid chromatography; SUV, small unilamellar vesicles; TFA, trifluoroacetic acid; TFE, 2,2,2-trifluoroethanol; TOCSY, total correlation spectroscopy; TRNOE, transferred NOE; TSP, 3-(trimethylsilyl) propionate, sodium salt; $T_1\rho$, spin−lattice, longitudinal relaxation time in the rotating frame; T_2, spin−spin, transverse relaxation time; 2D, two-dimensional; 3D, three-dimensional.

10.1021/bi991225t CCC: $18.00
Published on Web 10/26/1999

by two-dimensional transferred nuclear Overhauser enhancement (TRNOE) NMR experiments (*31*). The N-terminal (Leu 6−Leu 10) and C-terminal (Leu 13−Lys 21) segments assumed α-helical conformations and were connected via a less structured segment (Thr 11−Gly 12). The C-terminal Arg 22−Gln 26 segment that is α-helical in crystals, methanol, and micelles did not show an ordered conformation in the vesicle-bound state. In agreement with this observation, an amide-exchange analysis of melittin bound to bilayers of phosphatidylcholine and phosphatidylserine has shown that the four C-terminal residues do not have α-helical conformation (*32*).

The orientation of melittin in lipid bilayers depends on the kind of model membrane used (*33*). In a dry lipid membrane, polarized IR experiments suggested the existence of a transmembrane helix orientation (*34*−*36*). Results consistent with these findings have been provided by Smith et al. (*37*), who studied the carbonyl groups of ^{13}C-enriched melittin incorporated into bilayers of the diether lipid, ditetradecylphosphatidylcholine, aligned between stacked glass plates. These results were consistent with a helical conformation and a transbilayer orientation in the lipid membranes. However, when bound to fully hydrated bilayers, melittin is preferentially oriented parallel to the membrane. Spin-label EPR and ATR-FTIR results indicated that melittin binds at the interface with the helix approximately parallel to the plane of the membrane (*33*, *38*, *39*).

In a previous study, diastereomers (D-amino acids containing analogues) of melittin were synthesized and their function was investigated (*40*). These diastereomers lost their cytotoxic effect on mammalian cells, but retained their antibacterial activity and completely lysed both Gram-positive and Gram-negative bacteria. Melittin diastereomers bind to and destabilize only negatively charged phospholipid vesicles, in contrast to native melittin, which binds strongly to both negatively charged and zwitterionic phospholipids. The partition coefficient, the depth of penetration into the membrane, and the membrane-permeating activity of the diastereomers with negatively charged phospholipids were similar to those obtained with melittin.

To gain insight into the molecular mechanism of selective lysis of bacteria and negatively charged membranes by [D]-V^{5,8},I^{17},K^{21}-melittin (D-amino acids at positions V^{5,8},I^{17},K^{21}) and to further elucidate the mechanism of melittin folding and insertion into membranes, 2D-NMR and ATR-FTIR experiments were conducted. The structure of [D]-V^{5,8},I^{17},K^{21}-melittin was characterized in water, membrane-mimicking environment (TFE and methanol), and DPC/DMPG micelles.

EXPERIMENTAL PROCEDURES

Materials. 4-Methyl benzhydrylamine resin (BHA) and butyloxycarbonyl (Boc) amino acids were purchased from Calibochem-Novabiochem (La Jolla, CA). Other reagents used for peptide synthesis included trifluoroacetic acid (TFA, Sigma), *N*,*N*-diisopropylethylamine (DIEA, Aldrich, distilled over ninhydrin), dicyclohexylcarbodiimide (DCC, Fluka), 1-hydroxybenzotriazole (HOBT, Pierce) and dimethylformamide (peptide synthesis grade, Biolab). Egg phosphatidylcholine (PC) was purchased from Lipid Products (South Nutfield, U.K). Egg phosphatidylglycerol (PG) was purchased from Sigma. Deuterated compounds used for NMR sample preparation, 2,2,2-trifluroethanol-d_3 99.94% (TFE), methanol-d_4 99.96%, deuterium oxide 99.96%, and dodecylphosphocholine-d_{38} 98% (DPC) were purchased from Cambridge Isotope Laboratories (MA). 1,2 Dimyristoyl-*sn*-glycerol-3-d$_{54}$, sodium salt (DMPG), was purchased from Avanti Polar Lipids (Alabama), and methanol-d_3 98% was purchased from Carl Roth (Karlsruhe, Germany). All other reagents were of analytical grade.

Peptide Synthesis and Purification. Peptides were synthesized by a solid-phase method on a 4-methyl benzhydrylamine resin (BHA) (0.05 mequiv) (*41*). The resin-bound peptides were cleaved from the resins by hydrogen fluoride (HF) and extracted with dry ether after HF evaporation. HF cleavage of the peptides bound to 4-methyl benzhydrylamine resin resulted in C-terminus amidated peptides. These crude peptide preparations contained one major peak, as revealed by RP-HPLC, that was 60−80% pure peptide by weight. The synthesized peptides were further purified by RP-HPLC on a C_{18} reversed-phase Bio-Rad semipreparative column (250 × 10 mm, 300 Å pore size, 5 μm particle size). The column was eluted in 40 min, using a linear gradient of 10 to 60% acetonitrile in water, both containing 0.05% TFA (v/v), at a flow rate of 1.8 mL/min. The purified peptides, which were shown to be homogeneous (∼95%) by analytical HPLC, were subjected to amino acid analysis and fast atomic bombardment mass spectroscopy to confirm their composition and molecular weight.

Sample Preparation. Experiments on micelle samples were carried out at 323 and 318 K, and those in water, TFE/water, and methanol solutions at 287 and 277 K. The micelle samples used in the NMR experiments were prepared by dissolving 5.8 mg of [D]-V^{5,8},I^{17},K^{21}-melittin to a final concentration of 3.7 mM in water (90% H_2O and 10% D_2O) with perdeuterated DPC/DMPG (4:1, molar ratio) and with 0.05% NaN_3 to prevent bacterial growth. The pH of the sample was adjusted to 3.7 by the addition of small aliquots of DCl and NaOD. The TFE-d_3/water 40% (v/v), methanol-d_3, methanol-d_4, and water (90% H_2O and 10% D_2O) samples contained 3.0−4.4 mM peptide, with 0.05% NaN_3 at pH* = 3.3−3.9. Under these conditions, melittin in aqueous solution is found to be monomeric (*20*, *21*). The sample in TFE/water contained 10 mM sodium phosphate buffer.

NMR Measurements. 2D NMR spectra were measured at ^{1}H resonance frequencies of 500 and 600 MHz on Bruker DMX spectrometers in the phase-sensitive mode using the TPPI method (*42*). The carrier frequency was set on the HDO signal or on the OH signal in the methanol samples. Water and methanol suppression were achieved using the Watergate scheme (*43*), and for the methanol-d_4 samples, weak presaturating power was applied on the hydroxyl proton resonance during the relaxation delay. HOHAHA spectra (*44*) were measured using the WALTZ (*45*) pulse sequence with several mixing times ranging 34−100 ms. The NOESY experiments (*46*, *47*) were recorded with mixing times in the range 100−350 ms. DQF-COSY (*48*, *49*) spectra were measured by conventional procedures. The relaxation delay was 1.2 s in the HOHAHA experiments and 1.5 s in the NOESY experiments. Typically, 96−176 transients were collected for each increment of t_1 in the NOESY experiments, 32−78 in the HOHAHA experiment, and 118−200 in the DQF-COSY experiments. All experiments were recorded with a spectral width of 13 ppm, with 2048 or 8192 data points in the F_2 dimension, and 512 increments in the F_1

dimension. Natural abundance ^{13}C-decoupled HSQC (*50*) data was measured for the methanol-d_4 and DPC/DMPG micelle samples. The spectrum was folded in order to gain higher resolution, 4096 data points were collected in the F_2 dimension, and 256 increments were preformed in the F_1 dimension. The water signal was used as a ^{1}H reference for all the samples except for the methanol samples, in which the chemical shifts were determined relative to external TSP as 0.00 ppm (*51*). In addition, TSP also served as a standard for the ^{13}C chemical shift, in the HSQC experiments. The ^{13}C chemical shift value was calculated relative to 0.00 ppm (*52*).

$^3J_{HN\alpha}$ coupling constants were measured from HOHAHA spectra acquired with 8192 data points in the F_2 dimension and subsequently zero-filled to 16 384 (*53*). Lorentzian line shapes were fitted to the in-phase doublets, and $^3J_{HN\alpha}$ were derived only from reasonably good fits. The broadening of the amide proton resonances of the peptide in TFE and DPC/DMPG solutions prevented the determination of the *J*-coupling.

Spectra were processed with the XWINNMR software (Bruker Analytische Messtechnik GmbH) on a Silicon Graphics Indy R5000Sc workstation. Zero filling and a multiplication of the free induction decay by a shifted squared sine window function was applied in both dimensions prior to Fourier transformation.

NOE Measurements and Experimental Restraints. Spectra recorded at 287 K were used for determining the structure of [D]-V^{5,8},I^{17},K^{21}-melittin in water, TFE/water, and methanol solutions, and the spectra at 323 K were used for the DPC/DMPG micelle sample. The calibration for distance restraints was based on a typical distance of 3.5 Å for the C$^\alpha$H(i)/HN(i+1) cross-peak of the residues involved in α-helix (*54*). In the aromatic and HN/HN regions of the spectrum, the volume of a sequential HN(i)/HN(i+1) cross-peak in the α-helical region with a known distance of 2.8 Å was chosen as a reference. The distance between the β-methylene protons, which are 1.77 Å apart, was used as a reference for the NOE contacts in the aliphatic region of the spectrum.

The measured $^3J_{HN\alpha}$ coupling constants for the peptide in methanol were used to derive constraints for the ϕ angles along the peptide backbone. The ϕ angles were constrained between −80 and −40°, when $^3J_{HN\alpha} < 6$, the Chemical Shift Index (C.S.I) values were smaller than −0.2 ppm (*55*), and NOEs characteristics of a helical structure were observed. If only two of the above conditions were satisfied, the ϕ angle was set between −90 and −30°.

Structure Calculations. Structure calculations were performed using a standard hybrid distance geometry-simulated annealing protocol (*56*) with XPLOR v.3.1 program (*57*) on a Silicon Graphics Indy R5000Sc workstation. The structures were displayed for analysis on a Silicon Graphics workstation using the Insight II program (MSI Technologies, Inc.).

The resonances could not be assigned stereospecifically due to the lack of $^3J_{H_\alpha-H_\beta}$ and $^3J_{H_N-H_\beta}$ coupling parameters; therefore, the distance constraints were averaged according to $(\langle R_{ij}^{-6}\rangle)^{-1/6}$ (*58*−*60*). A correction of 0.5 Å was added to the upper limit of constraints involving a methyl group, and 1 Å was added to the upper limit of methyl−methyl constraints. The constraints were then classified into strong (1.8−2.5 Å), medium (1.8−3.5 Å), and weak (1.8−4.5 Å) and subjected to hybrid distance geometry-dynamical simulated annealing calculations (*56*). The NOE force constant was set to 50 kcal/mol for all calculations. After two rounds of simulated annealing refinement with 2000 cooling steps from 1000 to 100 K, initial low-resolution structures were obtained. These were used to complete the assignment of ambiguous NOE cross-peaks.

Structure determination by NMR is based on a large number of restraints on proton−proton distances, which are obtained from the analyses of the NOESY spectrum of the protein (*61*, *62*). In the study of [D]-V^{5,8},I^{17},K^{21}-melittin bound to DPC/DMPG micelles, a total of 322 distance restraints consisting of 10 long range, 81 medium range, and 231 short-range constraints were determined from the NOESY spectra. Structure calculations for [D]-V^{5,8},I^{17},K^{21}-melittin in methanol solution were done only for residues 12−26, which show a defined secondary structure. In this computation, a total of 170 distance restraints were used (39 long range, 29 medium range and 102 short range). No structure calculations of the peptide in TFE/water solution could satisfy the NOE constraints, probably due to the fact that the peptide does not exist in a single conformation in this solvent.

ATR-FTIR Measurements. Spectra were obtained with a Bruker equinox 55 FTIR spectrometer equipped with a deuterated triglyceride sulfate (DTGS) detector and coupled with an ATR device. For each spectrum, 200 or 300 scans were collected, with resolution of 2 cm^{-1}. During data acquisition, the spectrometer was continuously purged with dry N_2 to eliminate the spectral contribution of atmospheric water. Samples were prepared as previously described (*63*); briefly, a mixture of PC/PG (4:1 w/w, 0.66 mg) alone or with the peptide was deposited on a ZnSe horizontal ATR prism (80 × 7 mm). The aperture angle of 45° yielded 25 internal reflections. Prior to sample preparations, the trifluoroacetate (CF_3COO^-) counterions, which strongly associate to the peptide, were replaced with chloride ions through several lyophilizations of the peptide in 0.1 M HCl. This allowed the elimination of the strong C═O stretching absorption band near 1673 cm^{-1} (*64*). Lipid−peptide mixtures were prepared by dissolving in a 1:2 MeOH/CH_2Cl_2 mixture and drying under a stream of dry nitrogen while moving a Teflon bar back and forth along the ZnSe prism. Polarized spectra were recorded and the data for the respective pure phospholipid in each polarization were subtracted to yield the difference spectra. The background for each spectrum was a clean ZnSe prism. Hydration of the sample was achieved by the introduction of excess of deuterium oxide (^2H_2O) into a chamber placed on top the ZnSe prism in the ATR casting and incubation for 2 h prior to spectra acquisition. H/D exchange was considered complete on the basis of the complete shift of the amide II band. Any contribution of ^2H_2O vapor to the absorbance spectra near the amide I peak region was eliminated by subtraction of the spectra of pure lipids equilibrated with ^2H_2O under the same conditions. Prior to curve fitting, a straight baseline passing through the ordinates at 1700 and 1600 cm^{-1} was subtracted. To resolve overlapping bands, the spectra were processed using PEAKFIT (Jandel Scientific, San Rafael, CA) software. Second-derivative spectra accompanied by 13-data-point Savitsky-Golay smoothing were calculated to identify the frequencies of components of spectral bands.

Analysis of the Polarized ATR-FTIR Spectra. The ATR electric fields of incident light were calculated as follows (*65*, *66*):

$$E_z = \frac{2\sin\theta\sin\theta}{\sqrt{(1-n_{21}^2)[(1+n_{21}^2)\sin^2\theta - n_{21}^2]}}$$

$$E_x = \frac{2\cos\theta\sqrt{\sin^2\theta - n_{21}^2}}{(1-n_{21}^2)[(1+n_{21}^2)\sin^2\theta - n_{21}^2]}$$

$$E_y = \frac{2\cos\theta}{\sqrt{1-n_{21}^2}}$$

where θ is the angle light beam between the prism and the normal to the point of reflection (45°), and $n_{21} = n_2/n_1$, while n_1 and n_2 are the refractive indices of ZnSe and the membrane sample, assumed to be 2.4 and 1.5, respectively. Under these assumptions, E_x, E_y, and E_z are 1.09, 1.81, and 2.32, respectively. The dichroic ratio (A_p/A_s) is defined as the ratio between absorption of incident light polarized parallel to the membrane plane and perpendicularly to it. This ratio, together with the electric field components are used to calculate the orientation order parameter, *f*, by the following formula:

$$R^{ATR} = \frac{A_p}{A_s} = \frac{E_X^2}{E_Y^2} + \frac{\dfrac{E_Z^2}{E_Y^2}\left(f\cos^2\alpha + \dfrac{1-f}{3}\right)}{\dfrac{f\sin^2\alpha}{2} + \dfrac{1-f}{3}}$$

where α is the angle between the transition moment of the amide I vibration of an α-helix and the helix axis. Several values ranging 27−40° were reported for α in the literature (*67*). We used the values of 27° (*66*, *68*) and 39° (*69*, *70*) for α. Lipid order parameters were obtained from the symmetric (∼2853 cm^{-1}) and antisymmetric (∼2922 cm^{-1}) lipid stretching mode using the same equations, setting α = 90° (*66*).

RESULTS

Environment Selection for NMR Studies. The structure of [D]-$V^{5,8}$,I^{17},K^{21}-melittin was characterized in water as well as in the three membrane-mimicking environments; 40% 2,2,2-trifluoroethanol (TFE)/water solution, methanol, and DPC/DMPG micelles. The spectrum of [D]-$V^{5,8}$,I^{17},K^{21}-melittin exhibited very few peaks when measured in aqueous sample containing phosphate buffer, probably due to the line broadening resulting in cancellation of peaks. This may be attributed to the formation of tetrameric aggregates as occurs in melittin (*17*−*22*). The similar behavior of [D]-$V^{5,8}$,I^{17},K^{21}-melittin and melittin led us to carry out the experiments under conditions in which melittin was shown to be monomeric in both solutions and membrane phases (*2*). Alcohols (such as TFE and methanol) are used as membrane mimetic agents, due to their low dielectric constant. It was proposed (*71*) that alcohols stabilize the helical structure in melittin by direct hydrophobic interactions between the hydrophobic groups of alcohols and those of melittin. A TFE concentration of 30−50% is typically sufficient to allow peptides with helical propensities, especially amphipatic peptides, to form stable secondary structures in aqueous solution (*72*−*75*). In light of Oren and Shai results (*40*), negatively charged micelles were chosen for this study, a combination of DPC, which is a zwitterionic detergent, and DMPG, a negatively charged phospholipid. DPC is a commonly used detergent for solubilization of membrane peptides and proteins, because the small uniform micelles reorient rapidly enough for solution NMR spectroscopy (*76*). It was previously shown that complete binding of melittin to 1-palmitoyl-2-oleyl-*sn*-glycero-3-phosphocholine (POPC)/1-palmitoyl-2-oleoyl-*sn*-glycero-3-phosphoglycerol (POPG) (4:1 w/w) (*14*) was achieved at a molar ratio of 1:30. NMR studies have shown that melittin forms stoichiometrically well-defined mixed micelles with DPC (*77*) and 1-myristoyl-2-hydroxy-*sn*-glycero-3-phosphocholine (MMPC) (*78*) at a molar ratio of 1:40 and 1:30, respectively. In addition, a well-defined secondary structure of melittin was determined by ATR-FTIR in POPC/POPG (4:1 w/w) at a peptide:lipid molar ratio of ∼1:30 (*33*). On the basis of these studies, we carried out our experiments with the slightly lower ratio of peptide ([D]-$V^{5,8}$,I^{17},K^{21}-melittin) to detergent (DPC/DMPG) micelles of 1:50, to ensure complete partition of [D]-$V^{5,8}$,I^{17},K^{21}-melittin into the membranes. A similar ratio was used in the experiments done by Inagaki et al. (*29*) to determine the structure of melittin bound to perdeuterated DPC. Under these conditions, there was no doubling of peaks, indicating that at this detergent concentration all the peptide is bound to the micelle.

Resonance Assignment of the Peptide. The ^{1}H resonances in the NMR spectra of the peptide were assigned by the sequential assignment methodology developed by Wüthrich and co-workers (*61*), using NOESY and HOHAHA spectra measured consecutively and under the same conditions. First, the complete spin systems of the individual amino acid residues were identified using the HOHAHA spectra. Next, the backbone sequential connectivities were established by following the αN, *β*N, and NN cross-peaks of adjacent amino acids in the fingerprint and the NN region of the HOHAHA and NOESY spectra. Two measurements at different temperatures solved all problems of resonance overlap.

[D]-$V^{5,8}$,I^{17},K^{21}-melittin in aqueous solution showed no clear evidence of a preferred secondary structure, except for a few NH/NH (*i*,*i*+1) NOEs that were observed for residues 5−9 and 19−22 at 4 °C. Similar results were obtained in a ^{1}H NMR study of a monomeric melittin in aqueous solution revealing that monomeric melittin in aqueous solution is predominantly in a random coil form, with the fragments 5−9 and 14−20 more structured than the rest of the peptide (*20*). Short $d_{\alpha\alpha}$ and $d_{\delta\alpha}$ distances were not observed for the Leu−Pro sequence, suggesting the presence of a trans peptide bond (*54*). Furthermore, the presence of $d_{\delta N}^{PX}$ and $d_{\alpha N}^{PX}$ NOE cross-peaks supported this impression.

In the DPC/DMPG micelles sample, a reasonable HOHAHA spectrum could only be obtained at a relatively high temperature (323 K). At this temperature, magnetization transfer from the $H^{N\epsilon}$ of lysine to the other side-chain protons was not observed. In the NOESY spectrum, the correlations between all the backbone amide protons and $^1H^{\alpha}$ protons were detected. An unusual high-field chemical shift was obtained for the *γ*-methylene protons of Lys 23. This deviation was also observed by Inagaki (*29*) with native

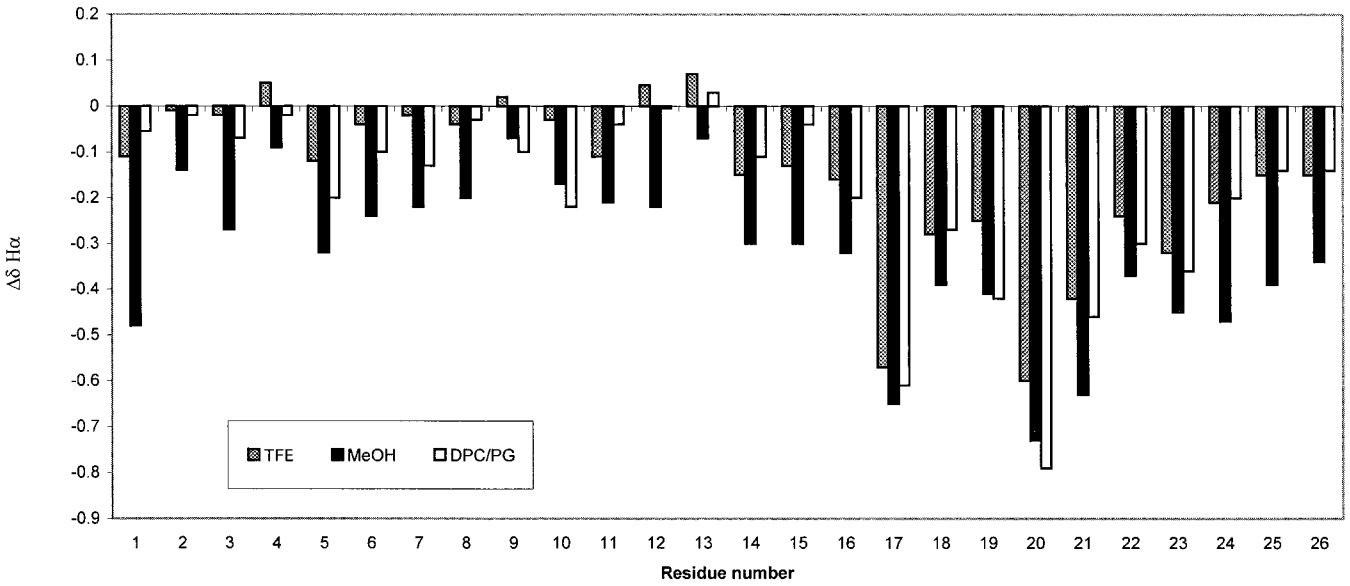

FIGURE 1: The deviation of the $^1H^\alpha$ chemical shifts from the random-coil values as a function of the residue number, for [D]-$V^{5,8}$,I^{17},K^{21}-melittin in TFE, methanol, and DPC/DMPG micelles. For the TFE/water sample random-coil values listed by Merutka et al. (*80*) were used, while for [D]-$V^{5,8}$,I^{17},K^{21}-melittin in methanol and DPC/DMPG micelles the random-coil values of Spera and Bax relative to TSP (*81*) were adopted.

melittin in DPC micelles. In both experiments, the aliphatic region was noisy, due to the fraction of undeuterated lipid remaining in the sample.

Secondary Structure Determination. It is well-known that the deviations of the chemical shifts from random-coil values are indicative of secondary structure. All residues experience a $^1H^\alpha$ upfield shift relative to the random-coil value when adopting a helical conformation and a downfield shift when found in an extended or β-stranded structure (*79*). On the other hand, C^α nuclei experience a downfield shift when they are located in helices and an upfield shift when they are located in β-strands (*52*). The $^1H^\alpha$ chemical shifts of [D]-$V^{5,8}$,I^{17},K^{21}-melittin in the TFE/water solution were compared to the random-coil chemical shifts in TFE/water solution tabulated by Merutka et al. (*80*). The $^1H^\alpha$ chemical shift of [D]-$V^{5,8}$,I^{17},K^{21}-melittin in methanol solution and DPC/DMPG micelles were compared to the random-coil chemical shift list in water of Wishart (*55*). The $^{13}C^\alpha$ and $^{13}C^\beta$ chemical shifts were compared to the random-coil values in water determined by Spera and Bax relative to TSP (*81*). Assuming that the random coil chemical shifts values are similar in methanol solution, no correction was applied for the values in methanol. The $^1H^\alpha$ chemical shifts were mostly derived from the HOHAHA experiments. In cases of overlap, these values were obtained from the ^1H-^{13}C correlated HSQC spectrum, which also served for evaluating the $^{13}C^\alpha$ and $^{13}C^\beta$ chemical shifts of [D]-$V^{5,8}$,I^{17},K^{21}-melittin in methanol and DPC/DMPG micelles.

In Figure 1, the deviations of the $^1H^\alpha$ chemical shifts from the random-coil values are seen for all three solvents. The largest upfield shifts are observed for residues located at the C-terminal part of the peptide. Moreover, it can be seen that [D]-$V^{5,8}$,I^{17},K^{21}-melittin in methanol has the highest helical tendency in this region, and the helix extends through more residues compared to the TFE/water and DPC/DMPG samples. Using a threshold value of −0.2 ppm, one can see that the helix in methanol extends from residue Pro 14 to the end of the peptide, while in the TFE/water and DPC/DMPG samples, the helix is between residues Ile 17 to Lys 23.

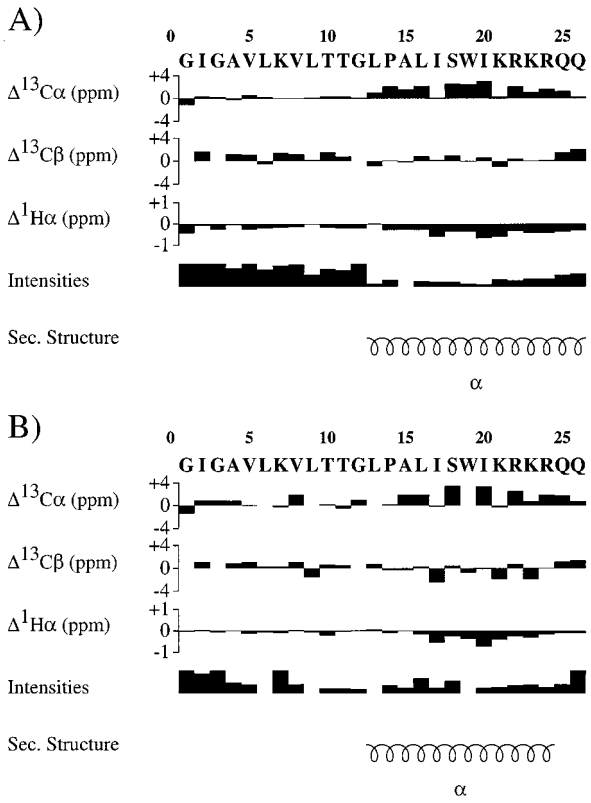

FIGURE 2: The diagrams of the absolute deviations of C^α, C^β, and H^α chemical shifts from their random-coil values and the secondary structure elements for (A) [D]-$V^{5,8}$,I^{17},K^{21}-melittin in methanol and B) [D]-$V^{5,8}$,I^{17},K^{21}-melittin in DPC/DMPG micelles. The random-coil values of Wishart (*55*), were used for calculating the $^1H^\alpha$ deviation, and for the $^{13}C^\alpha$ and $^{13}C^\beta$ the random-coil values estimated by Spera and Bax relative to TSP (*81*) were used. The relative intensities of the filled boxes correspond to the intensities measured from the spectra.

According to the $^{13}C^\alpha$ deviation (Figure 2), a well-defined helix from residue Leu 13 to Gln 26 is inferred for the peptide

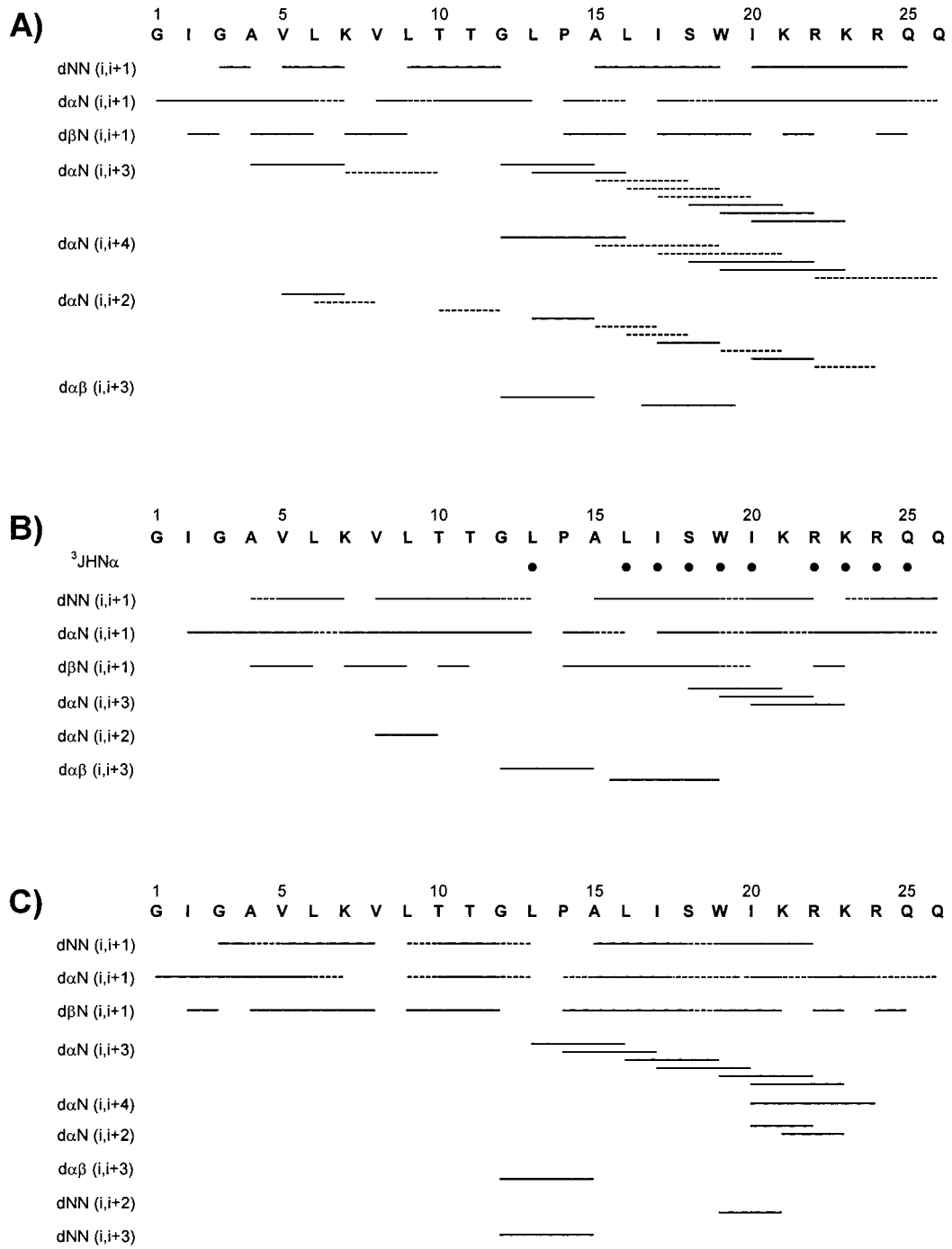

FIGURE 3: Schematic diagrams, summarizing the NOE connectivities observed for the peptide (A) in 40% TFE/water, (B) in methanol, and (C) in DPC/DMPG micelles. A dashed line indicates that the connectivity could not be determined due to an overlap of two or more cross-peaks. The slowly exchanging amides are shown with filled circles.

in methanol, while in the micelles, the helix is probably from residue Ala 15 to Gln 25. However, the deviation in the $^{13}C^{\alpha}$ chemical shift from random coil values was not observed for Ile 17 and Ile 21 in both spectra. These two residues are D-amino acids; consequently, they induce some flexibility in the α-helix, which is reflected in their chemical shift. The C^{β} chemical shifts values can only be used to identify stretches of β-strands and the identification of helices on the basis of these values is impossible (*52*, *81*). No β-strand region could be defined according to the C^{β} chemical shifts.

The chemical shift of Leu 6 and Leu 9 $^{13}C^{\alpha}$ in DPC/DMPG could not be distinguished in the HSQC spectra due to their identical $^{1}H^{\alpha}$ chemical shifts. In addition, no $^{1}H^{\alpha}/^{13}C^{\alpha}$ cross-peaks were observed for either Leu 13 or Trp 19. The disappearance of the peak for Leu 13 is probably due to the overlap with the water resonance. The disappearance of Trp 19 $^{1}H^{\alpha}$ chemical shift might be due to its restricted motion, resulting from its location in the micelle (*82*, *83*). Hence the T_2 and $T_{1\rho}$ relaxation times approach that of the micelle protons, and the substantial line broadening of this cross-peak causes its disappearance.

It is interesting to compare the $^{1}H^{\alpha}/^{13}C^{\alpha}$ cross-peaks intensities in the HSQC spectra of the C- and N-terminal segments. The cross-peaks of the N-terminal residues are stronger compared to those of the C-terminal residues. Since more mobile residues have longer T_2 and $T_{1\rho}$ relaxation times

(*84*), they give more intense cross-peaks than the peptide residues in the α-helix, which are less flexible.

NOE Connectivities. Figure 3 summarizes the NOE connectivities for [D]-V^{5,8},I^{17},K^{21}-melittin in the three samples. All three spectra show medium-range connectivities typical of α-helix in the C-terminal part of the peptide. No defined structure could be identified in the N-terminal segment. NH$_i$-NH$_{i+1}$ and C$^{\alpha}$H(i)/NH(i+1) NOE connectivities are spread throughout the entire peptide. But for the C-terminal half, a considerable number of αN(i,i+3) NOE cross-peaks together with a few αβ(i,i+3), αN(i,i+4), and NN(i,i+3) are observed. These NOEs are characteristic of a helical conformation (*61*). In addition, αN(i,i+2) and NN(i,i+2) connectivities characteristic of 3_{10}-helix are also detected.

Backbone Coupling Constant. Small $^3J_{HNH\alpha}$ coupling constants (<6 Hz) (*61*) are expected for regions of polypeptides with high helical content, while values larger than 7.5 Hz are expected for residues that are mostly in an extended conformation. The $^3J_{HNH\alpha}$ coupling constant values obtained for [D]-V^{5,8},I^{17},K^{21}-melittin in methanol are 6.0−7.4 Hz, for residues 2−12, indicating an averaging of different conformations. In contrast, for residues 13−25, small coupling constants are measured, characteristic of an α-helical structure. Due to an overlap of the Ala 15 and Gln 26 C$^{\alpha}$H(i)/NH(i+1) cross-peaks their coupling constants could not be measured.

Structure of [D]-V^{5,8},I^{17},K^{21}-Melittin in TFE/Water. The broad proton resonances in the TFE/water mixture prevents measurements of the $^3J_{HNH\alpha}$ coupling constant. The increase in the line width may be related to the viscosity of the mixture. This phenomenon of line broadening in TFE/water solution was also observed by Boisbouvier et al. (*85*) for Shiva-3, a cecropin-like synthetic peptide. In this solvent, [D]-V^{5,8},I^{17},K^{21}-melittin was found to be rather flexible as was indicated from calculating the ratio of $d_{\alpha N}(i,i)$ and $d_{N\alpha}(i,i+1)$ NOEs, $d_{N\alpha}/d_{\alpha N}$ (*86*). Since the NH(i)−C$^{\alpha}$H(i) and NH(i)−C$^{\alpha}$H(i−1) distances are fixed in α-helix and β-strand, the $d_{N\alpha}/d_{\alpha N}$ ratio larger than 1.1 represents a helix, and a ratio smaller than 0.83 represents a conformation in the β region conformational space. Measurements of this ratio for all possible residues in the peptide yielded values between 0.83 and 1.1, except for residues Leu 16, Ile 20, and Lys 21, which had $d_{N\alpha}/d_{\alpha N}$ ratio above 1.1. Thus there is no strong preference for either an α-helix or a β-strand conformation. Even though the NOE connectivities of the peptide seems to represent a helical structure, the measured $d_{NN}/d_{\alpha N}$ ratios were smaller than 1, indicating that the peptide conformation is averaged (*54*). Due to this conformational equilibrium, we could not calculate the peptide conformation from the NOE constraints derived from the TFE/water spectra.

Structure Calculation of [D]-V^{5,8},I^{17},K^{21}-Melittin in DPC/DMPG Micelles and in Methanol. A total of 81 refined structures with no NOE violations greater than 0.5 Å were calculated for the peptide in DPC/DMPG micelles. The rms deviation between the 24 lowest energy structures and the averaged structure is 1.0 Å for the backbone atoms of residues 13−23 and 3.5 and 4.1 Å for the backbone and all heavy atoms, respectively, of all peptide residues. The superposition of the 24 lowest energy structures (optimized for the backbone of residues 13−23) is shown in Figure 4. As expected from the NOE connectivities, the calculated structures do not converge in the N-terminal region, which was found to be more flexible. However, the C-terminal folds into a well-defined helical structure. As was observed by Inagaki (*29*) for melittin bound to DPC micelles, the side chain of Lys 23 is close to the indole ring of Trp 19, and as a result, the γ-protons of Lys 23 are shifted to a higher field.

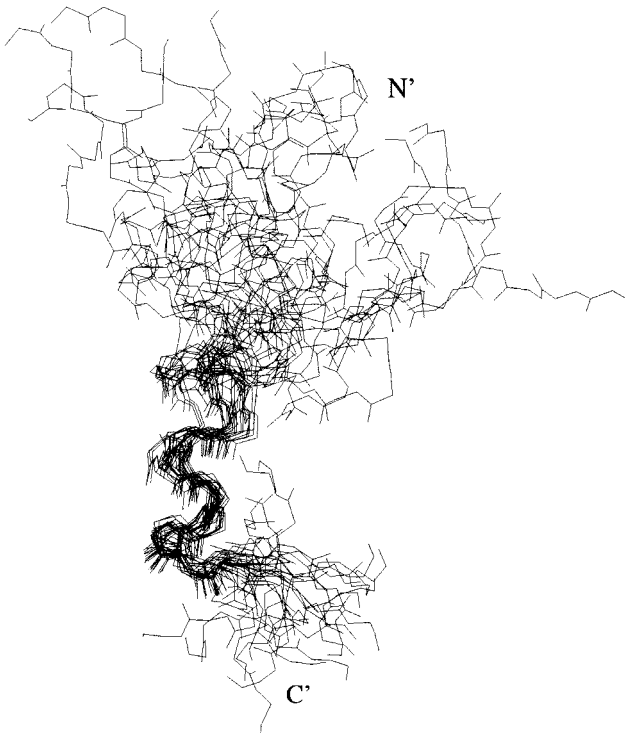

FIGURE 4: Superposition of backbone atoms for the 24 lowest energy structure solutions of [D]-V^{5,8},I^{17},K^{21}-melittin in DPC/DMPG micelles. The fit was optimized for the backbone of residues 13−23. The structures are superimposed on the lowest energy structure.

A total of 148 structures were calculated for [D]-V^{5,8},I^{17},K^{21}-melittin in methanol. The 27 lowest energy structures for residues 12−26 have no distance restraint violation greater than 0.5 Å. These structures are shown in Figure 5. They have been superimposed over the well-defined region from residues 13 to 23, and, for these residues, the rms difference from the average structure is 0.94 Å for the backbone atoms, and 3.37 Å for all the non-hydrogen atoms. As observed for DPC/DMPG micelles, the C-terminal half of the peptide forms a helix with a bend between residues 12 and 15.

Orientation of the Peptides in Lipid Multibilayers Determined by ATR-FTIR Spectroscopy. Polarized ATR-FTIR was used to determine the orientation of the peptides within lipid bilayers. The phospholipid composition (PC/PG 4:1 w/w) and peptide:lipid molar ratios (1:50) were similar to that used in the NMR experiments. Spectra of the amide I region of [D]-V^{5,8},I^{17},K^{21}-melittin and melittin bound to PC/PG (4:1 w/w) multibilayers are shown in Figure 6. The major component of the amide I band of both melittin and [D]-V^{5,8},I^{17},K^{21}-melittin is centered at 1645 cm^{-1}. The amide I spectra of melittin was symmetric in shape and appeared to be composed of one single major component, in agreement with previous findings (*33*). However, a second-derivative analysis of [D]-V^{5,8},I^{17},K^{21}-melittin spectra revealed minor components at 1666 and 1678 cm^{-1}. In principle, α-helical and unordered structures can contribute to the amide I vibration at almost identical wavenumbers in the range 1645−1650 cm^{-1}, and it is difficult to determine the precise proportion of α-helix and random-coil conformations from

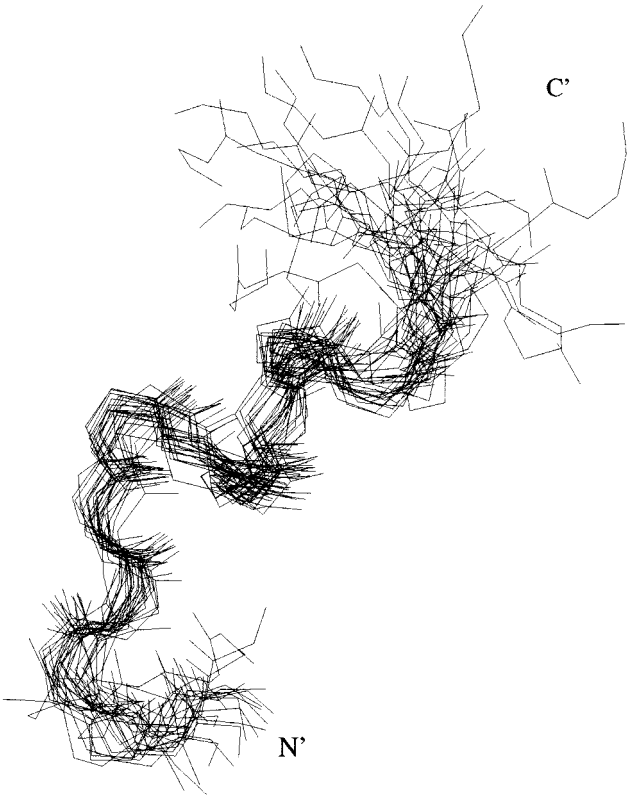

FIGURE 5: Superposition of the 27 lowest energy calculated structures for [D]-$V^{5,8}$,I^{17},K^{21}-melittin in methanol for residues 12−26. Only backbone atoms are shown. The structures were superimposed on the lowest energy structure, and the fit was optimized for the well-defined region between residues 13 and 23.

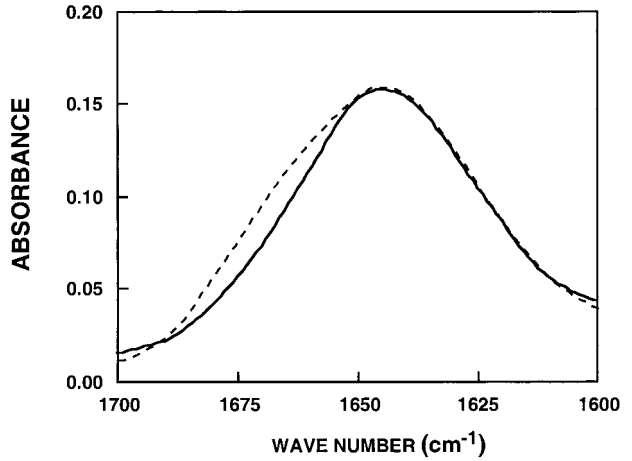

FIGURE 6: FTIR spectra of the amide I band (1700−1600 cm^{-1}) of melittin (continuous line) and [D]-$V^{5,8}$,I^{17},K^{21}-melittin (dashed line) bound to PC/PG (4:1 w/w) multibilayers. A 1:50 peptide:lipid molar ratio was used.

IR spectra (*33*). Therefore, no attempt was made to deconvolute the amide I spectra of the peptides into components, and the ATR-dichroic ratios were determined directly from the peak height at 1645 cm^{-1}. However, circular dichroism of melittin in lipid membranes and detergent revealed 70% α-helix and 30% random coil (*77*, *87*), and Raman spectroscopy showed that the fraction of α-helical residues of melittin in membrane is 76% (*88*). In addition, the results of this NMR study revealed that the fraction of helical residues of [D]-$V^{5,8}$,I^{17},K^{21}-melittin in micelles is ∼50%. With this additional information, the order parameter of the

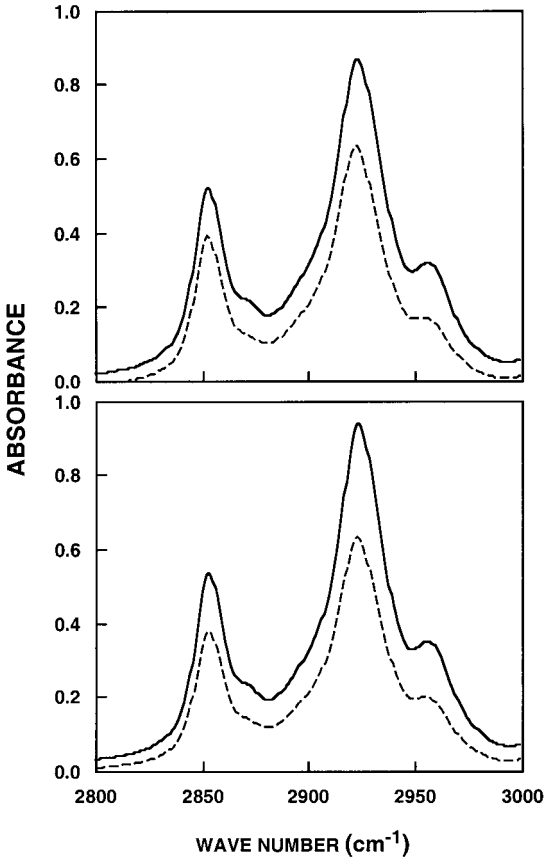

FIGURE 7: ATR dichroism spectra of parallel and perpendicular polarized ATR-FTIR absorbance spectra between 3000 and 2800 cm^{-1} for the lipid CH_2 symmetric and antisymmetric vibration of PC/PG multibilayers alone (A) and incorporated with [D]-$V^{5,8}$,I^{17},K^{21}-melittin (B). Peptide:lipid molar ratio was 1:50.

helical portion of melittin and [D]-$V^{5,8}$,I^{17},K^{21}-melittin, *f*, was calculated from the ATR-dichroic ratio of the amide I band.

The dichroic ratio values, *R*, were calculated from the amide I absorption at 1645 cm^{-1} in the polarized spectra and are 1.50 ± 0.02 and 1.47 ± 0.04 for [D]-$V^{5,8}$,I^{17},K^{21}-melittin and melittin, respectively. The corresponding order parameters assuming $\alpha = 27°$ (*66*, *68*) were calculated as described in Materials and Methods and are −0.17 and −0.18 for [D]-$V^{5,8}$,I^{17},K^{21}-melittin and melittin, respectively. When $\alpha = 39°$ (*69*, *70*), the order parameters are −0.28 and −0.30 for [D]-$V^{5,8}$,I^{17},K^{21}-melittin and melittin, respectively. Negative order parameters were observed for both peptides, typical of helices oriented nearly parallel to the membrane surface (*67*).

Orientation of the Phospholipid Membrane and the Effect of Melittin and [D]-$V^{5,8}$,I^{17},K^{21}-Melittin on Phospholipid Acyl-Chain Order. Polarized ATR-FTIR was used to determine the orientation of the lipid membrane. The symmetric [$\upsilon_{sym}(CH_2) \approx 2853$ cm^{-1}] and the antisymmetric [$\upsilon_{antisym}(CH_2) \approx 2922$ cm^{-1}] vibrations of lipid methylene C−H bonds are perpendicular to the molecular axis of a fully extended hydrocarbon chain. Thus, measurements of the dichroism of infrared light absorbance can reveal the order and orientation of the membrane sample relative to the prism surface. *R* value based on the stronger $\upsilon_{antisym}(CH_2)$ was 1.37 ± 0.02. A similar value ($R = 1.32$) was obtained when $\upsilon_{sym}(CH_2)$ was used instead (Figure 7A). On the basis of the

Table 1: ATR Dichroic Analysis of Phospholipid Multibilayers[a]

	peptide:lipid molar ratio	R of $\upsilon_{\text{antisym (CH}_2\text{)}}$	R of $\upsilon_{\text{sym (CH}_2\text{)}}$	$f\,\upsilon_{\text{antisym (CH}_2\text{)}}$	$f\,\upsilon_{\text{sym (CH}_2\text{)}}$
PC/PG		1.37 (±0.02)	1.32 (±0.02)	0.30 (±0.01)	0.32 (±0.01)
PC/PG + [D]-$V^{5,8}$,I^{17},K^{21}-melittin	1:50	1.45 (±0.02)	1.41 (±0.02)	0.25 (±0.01)	0.27 (±0.01)
PC/PG + [D]-$V^{5,8}$,I^{17},K^{21}-melittin	1:40	1.45 (±0.02)	1.41 (±0.02)	0.25 (±0.01)	0.27 (±0.01)
PC/PG + [D]-$V^{5,8}$,I^{17},K^{21}-melittin	1:30	1.46 (±0.03)	1.42 (±0.03)	0.25 (±0.01)	0.27 (±0.01)
PC/PG + [D]-$V^{5,8}$,I^{17},K^{21}-melittin	1:20	1.51 (±0.02)	1.47 (±0.02)	0.22 (±0.01)	0.24 (±0.01)
PC/PG + melittin	1:50	1.46 (±0.03)	1.42 (±0.03)	0.25 (±0.02)	0.27 (±0.02)
PC/PG + melittin	1:40	1.48 (±0.02)	1.43 (±0.02)	0.24 (±0.01)	0.26 (±0.01)
PC/PG + melittin	1:30	1.48 (±0.03)	1.43 (±0.03)	0.24 (±0.02)	0.26 (±0.02)
PC/PG + melittin	1:20	1.50 (±0.02)	1.45 (±0.02)	0.23 (±0.01)	0.25 (±0.01)

dichroic ratio of lipid stretching, the corresponding orientation order parameter, *f*, was calculated to be 0.30 (based on $\upsilon_{\text{antisym}}$) and 0.32 (based on υ_{sym}). Antisymmetric and symmetric peaks at ~2922 and ~2853 cm^{-1}, respectively, indicate that the membranes are predominantly in a liquid-crystalline phase (*66*, *89*). Thus, our data indicate that the lipid multibilayer used in the study was well oriented and in a liquid-crystalline phase. The effect of [D]-$V^{5,8}$,I^{17},K^{21}-melittin and melittin on the multibilayer acyl-chains order can be estimated by comparing the CH_2-stretching dichroic ratio of pure phospholipid multibilayers with that obtained with membrane-bound peptides. Figure 7 (panel B) shows an example of the ATR dichroism spectra of parallel and perpendicular polarized ATR-FTIR absorbance spectra between 2800 and 3000 cm^{-1} of PC/PG multibilayers incorporated with [D]-$V^{5,8}$,I^{17},K^{21}-melittin. The *R* values and the corresponding order parameters, *f*, at various peptide:lipid molar ratios ranging from 1:50 to 1:20 are summarized in Table 1. The data indicate that incorporation of the peptides into the membrane, even at high peptide:lipid molar ratio of 1:20, did not significantly change the lipid order. The data suggest that [D]-$V^{5,8}$,I^{17},K^{21}-melittin and melittin are surface localized and do not significantly destabilize the acyl-chain order. Interestingly, despite the differences in their structure, both peptides disrupt the acyl-chain order to the same extent.

DISCUSSION

The bee venom melittin is highly cytotoxic to both bacteria and mammalian cells, binding and destabilizing both negatively charged and zwitterionic phospholipid membranes. Contrary to melittin, its diastereomer containing four D-amino acids ($V^{5,8}$, I^{17}, and K^{21}) lyses bacteria but not erythrocytes, binding and destabilizing only negatively charged phospholipid membranes. To shed light onto these differences, 2D-NMR and ATR-FTIR spectroscopy were used to elucidate the influence of the four D-amino acids. The conformation of the peptide in four different environments, water, TFE/water and methanol solutions, DPC/DMPG micelles, and its orientation in PC/PG multibilayers, was studied and compared to native melittin.

On the basis of the NMR data, no clear presence of secondary structure was found for [D]-$V^{5,8}$,I^{17},K^{21}-melittin in water, in agreement with observations for native melittin (*20*). However, secondary structure determination revealed an amphipathic α-helix in the C-terminal region of [D]-$V^{5,8}$,I^{17},K^{21}-melittin in TFE/water and methanol solutions and in DPC/DMPG micelles. In methanol, the helix extends from residue Leu 13 to Gln 26, similar to the C-terminal helix of native melittin in methanol (*26*). A similar result was obtained in DPC/DMPG micelles, where the helix is from residue 13 to 24. The apparent disorder of the N-terminal reflects the flexibility of this region. Due to the few distance constraints determined from the NOSEY spectra for the N-terminal region, the calculated conformations do not converge.

A recent CD study on [D]-$V^{5,8}$,I^{17},K^{21}-melittin bound to large unilamellar phosphocholine vesicles (*90*) concluded that only about six residues are in an α-helical structure. One possible explanation for the large difference between the NMR and CD studies might be the different model systems in which the two studies were conducted. In the CD study, phosphocholine vesicles were used, whereas in the current NMR study TFE/water, methanol, and micelles were used. Comparison between the NMR structures of melittin in methanolic solution (*26*) and DPC micelles (*27*−*30*) and when bound to dipalmitoylglycerophosphocholine vesicles (*31*) reveals that the C-terminal Arg 22−Gln 26 segment is in an α-helical conformation in methanol and micelles, but it does not have an ordered conformation in the vesicle-bound state. These observed differences for melittin may also account for the observed differences in the conformation of [D]-$V^{5,8}$,I^{17},K^{21}-melittin in solution and when bound to micelle and vesicles. Another possible explanation may stem from the basic principles of secondary structure determination by the two methods. Circular dichroism in proteins is a phenomenon that occurs when chromophores (mainly nonbonding electrons of the carbonyl oxygens) in an asymmetrical environment interact with polarized light, while 2D-NMR conformation is determined by direct examination of the NOE between a given pair of atoms. The NOE is directly related to the inverse of the sixth power of the distance between the interacting nuclei. A diastereomer, as opposed to all L- or all D-amino acid peptides, is composed of both D- and L-amino acids that have opposite magnetic dipole moment and optical activity. The opposite circularly polarized absorption components of the D- and L-amino acids can cancel out and decrease the overall absorbance of the right-handed helix. In contrast to CD, the asymmetry of the amino acids does not affect secondary structure determination by NMR.

Polarized ATR-FTIR study of melittin and [D]-$V^{5,8}$,I^{17},K^{21}-melittin within hydrated negatively charged membranes indicated that the α-helical C-terminal region of the diastereomer is oriented nearly parallel to the membrane surface, similar to native melittin. Despite the difference in the structure of melittin and its diastereomer, both peptides did not significantly disrupt the acyl-chain order, even at high peptide:lipid molar ratios. These results further support our previous findings that the depth of penetration into the membrane, and the membrane-permeating activity of the diastereomer with negatively charged phospholipids are the

same as those obtained with melittin (*40*). The ATR-FTIR study indicated that the peptides are located at the interface, without deeply penetrating into the hydrophobic acyl-chain region, as was previously found for melittin (*39*). In any case, the unordered N-terminal of [D]-$V^{5,8}$,I^{17},K^{21}-melittin is most likely located at the interface because of the energetic cost of partitioning the peptide bonds into the hydrocarbon core, as was found for small hydrophobic peptides that cannot form secondary structures (*91*). Our results indicate that the N-terminal α-helix is not required for cytolytic activity toward bacteria. Similar conclusions were obtained in a recent study with a truncated α-helical analogue of pardaxin and its *β*-sheet diastereomer (*92*).

Previous studies have shown that the incorporation of a D-amino acid or even an adjacent pair of D-amino acids caused a local change in structure and flexibility and, therefore, affected the stability of α-helical structures (*93*−*95*, *102*). These findings are supported by the smaller downfield deviation of the $^{13}C^{\alpha}$ chemical shift seen for the two D-amino acids, Ile 17 and Ile 21, indicating some flexibility in the α-helix. Buckley et al. (*96*) showed that the C-terminal α-helix of melittin is more stable than the N-terminal α-helix in the presence of methanol/water mixture, and that the N-terminus was incompletely helical even in 100% methanol. These findings together with the influence of the D-amino acids incorporation may explain the disappearance of the N-terminal α-helix. An α-helical structure will remain without appreciable disturbance, despite the presence of a D-amino acid, in a segment with a high tendency to form a helical conformation (*97*), as in the case the C-terminal of melittin.

The results of the NMR and FTIR studies of [D]-$V^{5,8}$,I^{17},K^{21}-melittin enable us to gain insight into the stages involved in the folding and insertion of [D]-$V^{5,8}$,I^{17},K^{21}-melittin into the membrane, thus pointing out a possible molecular mechanism of the cell-selective activity. Little is known about the conformational changes following the insertion process of melittin into membranes. According to one model (*91*), the secondary structure of melittin is attained through sequential stages of interfacial binding in an unfolded state, secondary structure formation, and insertion of secondary structure units into the lipid bilayers, leading to disruption of the membrane. This model is supported by a study (*98*) that examined the conformational changes of melittin upon interaction with phospholipids. The results showed that melittin adsorbed on the lipid layer surface contains less α-helix than its counterpart inserted into the membrane. As the penetration depth of melittin is increased, more ordered structure (α-helix) appeared.

Factors affecting the free-energy cost of inserting unfolded peptides into both negatively charged and zwitterionic phospholipids membranes include the hydrophobic interactions between the nonpolar amino acids and the phospholipid hydrocarbon layer and the cost of partitioning the polar amino acids and the peptide bond (CONH) into a nonpolar environment (*99*). Electrostatic interactions appear to play an important role in the initial binding of the diastereomers to negatively charged membranes which are a major component of the bacterial membrane (*40*). When bound to negatively charged membranes, the positive charges of [D]-$V^{5,8}$,I^{17},K^{21}-melittin (+6) are partially neutralized by the negative charges of the phospholipid headgroups, thus reducing the energy cost of adsorbing the peptide into the membrane. Subsequently, it may allow the hydrophobic forces to manifest themselves following the formation of a stable α-helical structure in the C-terminal of the peptide, thus driving the peptide further into the interface, leading to membrane lysis.

In the case of zwitterionic phospholipids, the rate-limiting step of the insertion and membrane lysis appears to be the initial binding of [D]-$V^{5,8}$,I^{17},K^{21}-melittin to the surface, which is very low compared to native melittin (*100*). In a recent study (*90*), the free energies of transfer of melittin and [D]-$V^{5,8}$,I^{17},K^{21}-melittin from aqueous phase to the membrane of zwitterionic palmitoyloleoylphosphatidylcholine (POPC) were measured using equilibrium dialysis (*99*, *101*). The mole fraction partition coefficient K_X for [D]-$V^{5,8}$,I^{17},K^{21}-melittin and melittin was determined to be 80 (±30) and 4 (±2) × 10^5 respectively. This significant difference in the partitioning of the two peptides into zwitterionic phospholipids can account for the loss of the cytotoxic effect of the diastereomer on mammalian cells. The partitioning of native melittin into POPC was 5.0 ± 0.7 kcal/mol more favorable than the partitioning of [D]-$V^{5,8}$,I^{17},K^{21}-melittin. The free-energy difference between [D]-$V^{5,8}$,I^{17},K^{21}-melittin and melittin was consistent with the hypothesis that secondary structure formation is mainly driven by a reduction in the free energy of partitioning of peptide bonds caused by hydrogen bonding (*99*). In addition, it was shown that double D-amino acid replacement at the center of an α-helix destabilized the secondary structure by 4.5 kJ/mol (*102*). Since more energy has to be invested in the folding of [D]-$V^{5,8}$,I^{17},K^{21}-melittin compared to native melittin, it cannot readily form secondary structure in the surface and lower its free energy of transfer into the membrane (*90*). Hence, the peptide may be released from the zwitterionic membranes before it forms the α-helical structure. Alternatively, structural alteration of melittin due to the incorporation of D-amino acids may reduce the hydrophobic interactions that govern the partitioning into zwitterionic membranes, while exposing the positively charged amino acids, thus facilitating electrostatic interactions between the peptide and the membranes.

In summary, the results point at the role of secondary structure formation in selective cytolytic activity of [D]-$V^{5,8}$,I^{17},K^{21}-melittin. While the formation of N-terminal helix is not required for insertion into negatively charged membranes and cytolytic activity toward bacterial cells, it is a prerequisite for binding and insertion into zwitterionic membranes and hemolysis. Therefore, the diastereomers cannot form transmembrane pores in a "barrel-stave" mechanism, as has been proposed for the perturbation of the membrane bilayers by native melittin (*88*, *103*, *104*). The antimicrobial activity of the diastereomer seems to result from a pure lipid peptide interaction in a detergent like manner ["carpet-like" (*105*)]. Further understanding the properties of antimicrobial diastereomeric peptides in terms of their structure and membrane selectivity may aid in the design of new antimicrobial peptides and improved drugs to combat antibiotic-resistant pathogens.

ACKNOWLEDGMENT

We are greatly indebted to Yehezkiel Hayek for peptide purification, Vitali Tugarinov, Anat Zvi, and Tali Scherf for

their helpful contribution to the work and to Prof. Michael Levitt for most fruitful discussions.

SUPPORTING INFORMATION AVAILABLE

A table of the chemical shifts of [D]-$V^{5,8}$,I^{17},K^{21}-melittin in 40% (TFE)/water solution, methanol, and DPC/DMPG micelles and a list of constraints for the structure calculation of [D]-$V^{5,8}$,I^{17},K^{21}-melittin in DPC/DMPG micelles, and for structure calculation of [D]-$V^{5,8}$,I^{17},K^{21}-melittin in methanol for residues 12−26. This material is available free of charge via the Internet at http://pubs.acs.org.

REFERENCES

1. Habermann, E., and Jentsch, J. (1967) *Hoppe Seyler's Z. Physiol. Chem. 348*, 37−50.
2. Dempsey, C. E. (1990) *Biochim. Biophys. Acta 1031*, 143−161.
3. Habermann, E. (1980) in *Natural Toxins* (Eaker, D., and Wadstrom, T., Eds.) pp 173−181, Pergamon Press, New York.
4. Habermann, E. (1972) *Science 177*, 314−322.
5. Hider, R. C., Khader, F., and Tatham, A. S. (1983) *Biochim. Biophys. Acta 728*, 206−214.
6. Steiner, H., Hultmark, D., Engstrom, A., Bennich, H., and Boman, H. G. (1981) *Nature 292*, 246−248.
7. Blondelle, S. E., and Houghten, R. A. (1991) *Biochemistry 30*, 4671−4678.
8. Murata, M., Nagayama, K., and Ohnishi, S. (1987) *Biochemistry 26*, 4056−4062.
9. Ohki, S., Marcus, E., Sukumaran, D. K., and Arnold, K. (1994) *Biochim. Biophys. Acta 1194*, 223−232.
10. Mollay, C., and Kreil, G. (1974) *FEBS Lett. 41*, 141−144.
11. Dufourcq, J., and Faucon, J. F. (1977) *Biochim. Biophys. Acta 467*, 1−11.
12. Batenburg, A. M., van, E. J., Leunissen, B. J., Verkleij, A. J., and de-Kruijff. B. (1987) *FEBS Lett. 223*, 148−154.
13. Batenburg, A. M., Hibbeln, J. C., Verkleij, A. J., and de-Kruijff, B. (1987) *Biochim. Biophys. Acta 903*, 142−154.
14. Beschiaschvili, G., and Seelig, J. (1990) *Biochemistry 29*, 52−58.
15. Lafleur, M., Samson, I., and Pezolet, M. (1991) *Chem. Phys. Lipids 59*, 233−244.
16. Pott, T., Paternostre, M., and Dufourc, E. J. (1998) *Eur. Biophys. J. 27*, 237−245.
17. Gauldie, J., Hanson, J. M., Rumjanek, F. D., Shipolini, R. A., and Vernon, C. A. (1976) *Eur. J. Bichem. 61*, 369−376.
18. Faucon, J. F., Dufourcq, J., and Lussan, C. (1979) *FEBS Lett. 102*, 187−190.
19. Talbot, J. C., Dufourcq, J., de, B. J., Faucon, J. F., and Lussan, C. (1979) *FEBS Lett. 102*, 191−193.
20. Lauterwein, J., Brown, L. R., and Wüthrich, K. (1980) *Biochim. Biophys. Acta 622*, 219−230.
21. Brown, L. R., Lauterwein, J., and Wüthrich, K. (1980) *Biochim. Biophys. Acta 622*, 231−244.
22. Quay, S. C., and Tronson, L. P. (1983) *Biochemistry 22*, 700−707.
23. Dawson, C. R., Drake, A. F., Helliwell, J., and Hider, R. C. (1978) *Biochim. Biophys. Acta 510*, 75−86.
24. Knoppel, E., Eisenberg, D., and Wickner, W. (1979) *Biochemistry 18*, 4177−4181.
25. Terwilliger, T. C., Weissman, L., and Eisenberg, D. (1982) *Biophys. J. 37*, 353−361.
26. Bazzo, R., Tappin, M. J., Pastore, A., Harvey, T. S., Carver, J. A., and Campbell, I. D. (1988) *Eur. J. Biochem. 173*, 139−146.
27. Brown, L. R., and Wüthrich, K. (1981) *Biochim. Biophys. Acta 647*, 95−111.
28. Brown, L. R., Braun, W., Kumar, A., and Wüthrich, K. (1982) *Biophys. J. 37*, 319−328.
29. Inagaki, F., Shimada, I., Kawaguchi, K., Hirano, M., Terasawa, I., Ikura, T., and Go, N. (1989) *Biochemitry 28*, 5985−5991.
30. Ikura, T., Go, N., and Inagaki, F. (1991) *Proteins 9*, 81−89.
31. Okada, A., Wakamatsu, K., Miyazawa, T., and Higashijima, T. (1994) *Biochemistry 33*, 9438−9446.
32. Dempsey, C. E., and Butler, G. S. (1992) *Biochemistry 31*, 11973−11977.
33. Frey, S., and Tamm, L. K. (1991) *Biophys. J. 60*, 922−930.
34. Vogel, H., Jahnig, F., Hoffmann, V., and Stumpel, J. (1983) *Biochim. Biophys. Acta 733*, 201−209.
35. Brauner, J. W., Mendelsohn, R., and Prendergast, F. G. (1987) *Biochemistry 26*, 8151−8158.
36. Weaver, A. J., Kemple, M. D., Brauner, J. W., Mendelsohn, R., and Prendergast, F. G. (1992) *Biochemistry 31*, 1301−1313.
37. Smith, R., Separovic, F., Milne, T. J., Whittaker, A., Bennett, F. M., Cornell, B. A., and Makriyannis, A. (1994) *J. Mol. Biol. 241*, 456−466.
38. Altenbach, C., Froncisz, W., Hyde, J. S., and Hubbell, W. L. (1989) *Biophys. J. 56*, 1183−1191.
39. Kleinschmidt, J. H., Mahaney, J. E., Thomas, D. D., and Marsh, D. (1997) *Biophys. J. 72*, 767−778.
40. Oren, Z., and Shai, Y. (1997) *Biochemistry 36*, 1826−1835.
41. Merrifield, R. B., Vizioli, L. D., and Boman, H. G. (1982) *Biochemistry 21*, 5020−5031.
42. Marion, D., and Wüthrich, K. (1983) *Biochem. Biophys. Res. Commun. 113*, 967−974.
43. Piotto, M., Saudek, V., and Sklenar, V. (1992) *J. Biomol. NMR 2*, 661−665.
44. Davis, D. G., and Bax, A. (1985) *J. Am. Chem. Soc. 107*, 2820−2821.
45. Shaka, A. J., Keeler, J., Frenkiel, T. A., and Freeman, R. (1983) *J. Magn. Reson. 51*, 447−452.
46. Kumar, A., Wagner, G., Ernst, R. R., and Wüthrich, K. (1980) *Biochem. Biophys. Res. Commun. 96*, 1156−1163.
47. Macura, S., and Eenst, R. R. (1981) *Mol. Phys. 41*, 95−117.
48. Braun, W., Bosch, C., Brown, L. R., and Wüthrich, K. (1981) *Biochim. Biophys. Acta 667*, 377−396.
49. Piantini, U., and Sorensen, O. (1982) *J. Am. Chem. 104*, 6800−6801.
50. Sorensen, O. W., and Ernst, R. R. (1983) *J. Magn. Reson. 51*, 447−452.
51. Clore, G. M., and Gronenborn, A. M. (1994) *Methods Enzymol. 239*, 349−363.
52. Wishart, D. S., and Sykes, B. D. (1994) *J. Biomol. NMR 4*, 171−180.
53. Driscoll, P. C., Clore, G. M., Beress, L., and Gronenborn, A. M. (1989) *Biochemistry 28*, 2178−2187.
54. Wüthrich, K., Billeter, M., and Braun, W. (1984) *J. Mol. Biol. 180*, 715−740.
55. Wishart, D. S., Bigam, C. G., Holm, A., Hodges, R. S., and Sykes, B. D. (1995) *J. Biomol. NMR 5*, 67−81.
56. Nilges, M., Gronenborn, A. M., Brunger, A. T., and Clore, G. M. (1988) *Protein Eng. 2*, 27−38.
57. Brunger, A. T. (1992) *XPLOR 3.1 Manual*, New Haven, CT.
58. Brunger, A. T., Clore, G. M., Gronenborn, A. M., and Karplus, M. (1986) *Proc. Natl. Acad. Sci. U.S.A. 83*, 3801−3805.
59. Levy, R., Assulin, O., Scherf, T., Levitt, M., and Anglister, J. (1989) *Biochemistry 28*, 7168−7175.
60. Constantine, K. L., Madrid, M., Banyai, L., Trexler, M., Patthy, L., and Llinas, M. (1992) *J. Mol. Biol. 223*, 281−298.
61. Wüthrich, K. (1986) *NMR of Proteins and Nucleic Acids*, John Wiley, New York.
62. Wüthrich, K. (1989) *Acc. Chem. Res. 22*, 36−44.
63. Gazit, E., Miller, I. R., Biggin, P. C., Sansom, M. S. P., and Shai, Y. (1996) *J. Mol. Biol. 258*, 860−870.
64. Surewicz, W. K., Mantsch, H. H., and Chapman, D. (1993) *Biochemistry 32*, 389−394.
65. Harrick, N. J. (1967) *Internal Reflection Spectroscopy*, Interscience, New York.
66. Ishiguro, R., Kimura, N., and Takahashi, S. (1993) *Biochemistry 32*, 9792−9797.
67. Tamm, L. K., and Tatulian, S. A. (1997) *Q. Rev. Biophys. 30*, 365−429.
68. Rothschild, K. J., and Clark, N. A. (1979) *Science 204*, 311−312.
69. Tsuboi, M. (1962) *J. Polymer Sci. 59*, 139−153.

70. Bradbury, E. M., Brown, L., Downie, A. R., Elliott, A., Fraser, R. D. B., and Hanby, W. E. (1962) *J. Mol. Biol 5*, 230−247.
71. Hirota, N., Mizuno, K., and Goto, Y. (1998) *J. Mol. Biol. 275*, 365−378.
72. Lau, S. Y., Taneja, A. K., and Hodges, R. S. (1984) *J. Chromatogr. 317*, 129−140.
73. Nelson, J. W., and Kallenbach, N. R. (1989) *Biochemistry 28*, 5256−5261.
74. Lehrman, S. R., Tuls, J. L., and Lund, M. (1990) *Biochemistry 29*, 5590−5596.
75. Sonnichsen, F. D., Van, E. J., Hodges, R. S., and Sykes, B. D. (1992) *Biochemistry 31*, 8790−8798.
76. McDonnell, P. A., and Opella, S. J. (1993) *J. Magn. Reson. 55*, 301−315.
77. Lauterwein, J., Bosch, C., Brown, L. R., and Wüthrich, K. (1979) *Biochim. Biophys. Acta 556*, 244−264.
78. Yuan, P., Fisher, P. J., Prendergast, F. G., and Kemple, M. D. (1996) *Biophys. J. 70*, 2223−2238.
79. Wishart, D. S., Sykes, B. D., and Richards, F. M. (1991) *J. Mol. Biol. 222*, 311−333.
80. Merutka, G., Dyson, H. J., and Wright, P. E. (1995) *J. Biomol. NMR 5*, 14−24.
81. Spera, S., and Bax, A. (1991) *J. Am. Chem. Soc. 113*, 5490−5492.
82. Sui, S. F., Wu, H., Guo, Y., and Chen, K. S. (1994) *J. Biochem. Tokyo 116*, 482−487.
83. Ghosh, A. K., Rukmini, R., and Chattopadhyay, A. (1997) *Biochemistry 36*, 14291−14305.
84. Zvi, A., Kustanovich, I., Feigelson, D., Levy, R., Eisenstein, M., Matsushita, S., Richalet Secordel, P., Regenmortel, M. H., and Anglister, J. (1995) *Eur. J. Biochem. 229*, 178−187.
85. Boisbouvier, J., Prochnicka-Chalufour, A., Nieto, A. R., Torres, J. A., Nanard, N., Rodriguez, M. H., Possani, L. D., and Delepierre, M. (1998) *Eur. J. Biochem. 257*, 263−273.
86. Campbell, A. P., Sykes, B. D., Norrby, E., Assa Munt, N., and Dyson, H. J. (1996) *Folding Des. 1*, 157−165.
87. Vogel, H. (1981) *FEBS Lett. 134*, 37−42.
88. Vogel, H., and Jahnig, F. (1986) *Biophys. J. 50*, 573−582.
89. Cameron, D. G., Casal, H. L., Gudgin, E. F., and Mantsch, H. H. (1980) *Biochim. Biophys. Acta 596*, 463−467.
90. Ladokhin, A. S., and White, S. H. (1999) *J. Mol. Biol. 285*, 1363−1369.
91. Jacobs, R. E., and White, S. H. (1989) *Biochemistry 28*, 3421−3437.
92. Oren, Z., Hong, J., and Shai, Y. (1999) *Eur. J. Biochem. 259*, 360−369.
93. Krause, E., Beyermann, M., Dathe, M., Rothemund, S., and Bienert, M. (1995) *Anal. Chem. 67*, 252−258.
94. Rothemund, S., Beyermann, M., Krause, E., Krause, G., Bienert, M., Hodges, R. S., Sykes, B. D., and S, o. F. (1995) *Biochemistry 34*, 12954−12962.
95. Rothemund, S., Krause, E., Beyermann, M., Dathe, M., Engelhardt, H., and Bienert, M. (1995) *J. Chromatogr. A 689*, 219−226.
96. Buckley, P., Edison, A. S., Kemple, M. D., and Prendergast, F. G. (1993) *J. Biomol. NMR 3*, 639−652.
97. Gurunath, R., and Balaram, P. (1994) *Biochem. Biophys. Res. Commun. 202*, 241−245.
98. Sui, S. F., Wu, H., Guo, Y., and Chen, K. S. (1994) *J. Biochem. (Tokyo) 116*, 482−487.
99. Wimley, W. C., and White, S. H. (1996) *Nature Struct. Biol. 3*, 842−848.
100. Oren, Z., Hong, J., and Shai, Y. (1997) *J. Biol. Chem. 272*, 14643−14649.
101. Wimley, W. C., and White, S. H. (1993) *Anal. Biochem. 213*, 213-217.
102. Rothemund, S., Krause, E., Beyermann, M., Bienert, M., Sykes, B. D., and Sonnichsen, F. D. (1996) *Biopolymers 39*, 207−219.
103. DeGrado, W. F., Musso, G. F., Lieber, M., Kaiser, E. T., and Kezdy, F. J. (1982) *Biophys. J. 37*, 329−338.
104. Tosteson, M. T., and Tosteson, D. C. (1981) *Biophys. J. 36*, 109−116.
105. Oren, Z., and Shai, Y. (1998) *Biopolymers 47*, 451−463.

BI991225T